Electropolymerized Polyaniline Nanocomposites from Multi-Walled Carbon Nanotubes with Tuned Surface Functionalities for Electrochemical Energy Storage

Huige Wei,[a,b] Hongbo Gu,[a] Jiang Guo,[a] Suying Wei,[b,z] and Zhanhu Guo[a,*,z]

[a]*Integrated Composites Laboratory (ICL), Dan F. Smith Department of Chemical Engineering, Lamar University, Beaumont, Texas 77710, USA*
[b]*Department of Chemistry and Biochemistry, Lamar University, Beaumont, Texas 77710, USA*

The effects of the surface functional groups on the electrochemical properties and electrochemical energy storage were systematically studied by employing the as-received multi-walled carbon nanotubes (MWNTs) and two other MWNTs modified with ether and carboxylic acid functionalities (-C-O-C and -COOH), and ester functional groups (–COOR). The structure and morphology of the films prepared by electropolymerizing aniline onto MWNTs- coated carbon paper substrate were characterized by scanning electron microscopy and Fourier transform infrared spectroscopy. The band gaps obtained from ultraviolet–visible spectroscopy suggested slight difference in the structure of the nanocomposite films induced by the functional groups in the MWNTs. Electrochemical measurements revealed that all the nanocomposite films with MWNTs exhibited an enhanced capacitance compared to the film grown onto pure carbon paper. An energy density as high as 30 μWh/cm^2 corresponding to a power density of around 8 mW/cm^2 was obtained even at a high current density of 20 mA/cm^2 for the nanocomposite films. An equivalent circuit consisting of a combined resistance and a capacitor is well fitted with the electrochemical impedence spectroscopy data. Stability study showed that the nanocomposite films retained around 80% of the discharge capacity even after 1000 charge-discharge cycles, rendering these films promising for supercapacitor applications.

Due to the growing concerns over the fossil fuel usage, in terms of energy depletion and dramatic climate changes caused by massive carbon dioxide emissions, the development of sustainable and renewable energy storage resources with both high power density and large energy density has become an imperative demand.[1–3] Electrochemical capacitors (ECs) have attracted intense interest due to their potential for green transportation and large scale energy storage. Owing to their advantages of high energy density and power density as well as long cycle life,[4,5] ECs have great potential for filling the gap between batteries and conventional electrostatic capacitors, and they have versatile applications for portable electronics, hybrid electric vehicles, and large industrial equipments.[6] Based on different charge storage mechanisms, two types of ECs have been proposed: electric double layer capacitors (EDLCs, or ultracapacitors) and pseudocapacitors (or supercapacitors).[7] For EDLCs, only ion adsorption/desorption takes place between the interfaces of electrodes and electrolyte without Faradic process. Carbon materials with large specific surface area (SSA) including activated carbons (ACs),[8] carbon nanotubes (CNTs),[9] ordered mesoporous carbons (OMCs), and grapheme nanosheets (GNS) are usually employed to achieve EDLCs.[10,11] EDLCs are well known for their high power density (>10 KW/Kg) and long cycle life (>10^6 cycles).[12] However, the challenges are the low energy density (<5 Kh/kg)[6,13] and much lower areal capacitance (capacitance per unit area) ranging from 10–40 μF cm^{-2} due to both low density and gravimetric capacitance (capacitance per unit mass).[14] For pseudocapacitors or supercapacitors based on Faradic processes, the energy storage is achieved by electron transfer that follows reduction-oxidation (redox) reactions in the material. Transition metal oxides such as MnO_2,[15] RuO_2,[16] MoO_3,[17] Co_3O_4[18] and VO_x[19] and electrically conducting polymers such as polythiophenes (PThs),[20,21] poly(pyrrole),[22,23] poly(DNTD),[24,25] and poly(aniline) (PANI) have been been utilized for designing ECs. However, the problem regarding transition metal oxides is the low power density originating from their relatively high electrical resistance. On the contrast, conducting polymers exhibit relatively high conductivity and low cost compared to the carbon-based electrode materials. More

importantly, conducting polymers possess much higher gravimetric capacitance via pseudocapacitive redox reactions, making them feasible to increase the areal capacitance while keeping similar or even thinner films as those of the conventional carbon-based materials. Unfortunately, mechanical degradation of the electrode and fading electrochemical performance caused by the swelling and shrinking during the cycling redox reactions of conducting polymers limit their applications as electrochemical capacitors.[26]

For applications including small scale electronics and stationary energy storage devices where areal capacitance is a better indicator of the performance of supercapacitors than gravimetric capacitance, although the latter has always been used in the literature for comparison of the supercapacitor performance.[27,28] A strategy to combine faradaic pesudocapacitive conducting polymers and EDLs systems has been developed to obtain electrochemical capacitors with desirable properties.[29] Among various conducting polymers, PANI has received special attention because of its intriguing properties such as facile polymerization in aqueous media[30–33] or non-aqueous media,[34] good stability in air, low cost, and high conductivity. In the previous study, PANI nanocomposite films incorporated with tungsten oxide or graphite oxide have been electropolymerized onto indium tin oxide (ITO) coated glass slides to study the energy storage and electrochromic properties.[35,36] Although the stability of the films is enhanced, there are still challenges remaining, for example, a decreased areal capacitance resulting from the reduced amounts of aniline monomers electropolymerized, which is caused by the increased resistance brought by the tungsten oxide or graphite oxide coatings onto ITO.

Carbon nanotubes are considered as potentially revolutionary nanomaterials for electronic and energy storage devices due to their highly accessible surface area, nano-scale structure and good electrical conductivity.[37] Significant progress has been made in designing and preparing PANI/CNTs composites or thin films by in situ electropolymerization or chemical oxidative polymerization approaches for supercapacitor applications.[38,39] The excellent conducting properties of CNTs and their available mesoporosity are found to allow good charge propagation in the composites and therefore improve their capacitive performances.[40] Although many efforts have been put into the study of electrochemical properties using different types

*Electrochemical Society Active Member.
[z]E-mail: zhanhu.guo@lamar.edu; suying.wei@lamar.edu

of electrolyte or cell configuration (two-electrode or three-electrode method), the effects of different functionalities in the CNTs on the capacitive performances of the composites have not been reported.

In this work, freestanding PANI nanocomposite thin films grown onto MWNTs-coated carbon paper substrate were fabricated via electropolymerization technique from aqueous solutions and used directly both as the electrode and current collector. Three kinds of MWNTs, i.e., as-received and two modified including one with ether and carboxylic acid functionalities (-C-O-C and -COOH) and the other one with ester functional groups (–COOR), respectively, were employed to investigate on how the functional groups would affect the capacitive performances of the electrodes. The structure and morphology of the nanocomposite thin films were characterized by scanning electron microscopy (SEM) and Fourier transform infrared spectroscopy (FT-IR). The electrochemical performances of the nanocomposite films were investigated by cyclic voltammetry (CV), galvanostatic charge-discharge measurement, and electrochemical impedance spectroscopy (EIS) techniques. The effect of different substrates on the electrochemical performances of the thin films was studied. An equivalent circuit of the nanocomposite thin films was also proposed to fit the EIS data for a fundamental understanding of the capacitive behavior.

Experimental

Materials.— Aniline (C_6H_7N) and sulfuric acid (H_2SO_4, 95.0%–98.0%) was purchased from Sigma Aldrich. The carbon paper was provided by ElectroChem, Inc. MWNTs (SW*e*NT SMW 200X, average diameter: 10.4 nm; average length: 4.3 μm) were provided by SouthWest NanoTechnologies, Inc. The Modified MWNTs with different functionalities were prepared according to the method reported previously.[41] All the chemicals were used as received without any further treatment.

Preparation of CNTs/PANI nanocomposite thin film electrodes.— The freestanding MWNTs/PANI nanocomposite thin films were prepared via the electropolymerization of aniline monomers onto pure or modified MWNTs-coated carbon paper (CP). Three types of MWNTs, i.e., the as-received and two other modified including one with ether and carboxylic acid functionalities and the other one with ester functional groups, respectively, were dispersed in ethanol solvent and drop casted onto CP substrate and dried overnight in a fume hood before the elecctropolymerization. The four corresponding nanocomposite thin films obtained were denoted as PANI-CP, PANI-AS, PANI-EC, and PANI-E, respectively. The electropolymerization of aniline monomers was performed on an electrochemical working station VersaSTAT 4 potentiostat (Princeton Applied Research) in air. A typical electrochemical cell consisting of a reference electrode, a working electrode, and a counter electrode was employed. A saturated calomel electrode (SCE) electrode served as the reference electrode and a platinum (Pt) wire as the counter electrode. The CP substrate with an effective geometric area of about 3.5 cm^2 served as the working electrode. A typical electrochemical polymerization was performed 15 cycles scanned back and forth from 0 to +1.0 V vs. SCE at a scan rate of 50 mV/s in 1.0 M H_2SO_4 aqueous solution containing 0.1 M aniline monomers. The freestanding nanocomposite thin films obtained were used directly as the supercapacitor electrodes and current collectors.

Characterizations.— The morphology of the nanocomposite films was observed by a JSM-6700F system with a JEOL field emission scanning electron microscope (SEM). FT-IR spectrometer coupled with an ATR accessory (Bruker Inc. Vector 22) was used to characterize the surface functionality of the nanocomposites in the range of 500 to 4000 cm^{-1} at a resolution of 4 cm^{-1}. The optical properties were characterized using ultraviolet-visible diffuse reflectance spectroscopy techniques (Jasco V-670 spectrophotometer).

The electrochemical properties including CV, galvanostatic charge-discharge measurements, and electrochemical impedance spectroscopy (EIS) techniques were evaluated using a three electrode configuration. The CV was scanned from −0.2 to 0.8 V vs. SCE at a series of scan rates in 1.0 M H_2SO_4 aqueous solution. EIS was carried out in the frequency range of 100, 000 to 0.01 Hz at a 5 mV amplitude referring to the open circuit potential. The stability of the composites was also assessed using charge-discharge measurements at a current density of 50 mA/cm^2. All the characterizations were carried out at room temperature in air.

Results and Discussion

Electropolymerization of PANI on MWNTs modified carbon paper substrate characterizations.— Figure 1a–1d shows the growth of the PANI films onto different substrates by sweeping the potential from 0 to +1.0 V at a scan rate of 50 mV s^{-1} in an aqueous solution containing 0.1 M aniline and 1.0 M H_2SO_4. The aniline monomers can be readily electropolymerized onto the substrate with an observed increased current when the potential was increases to around +0.8 V. The increase current is due to the oxidation of aniline monomers and the initiation of the electropolymerization of PANI in the first cycle,[42] and the film growth can be confirmed by the current increase with increasing the CV cycles. The nanocomposite films exhibit similar CV patterns except of a significantly higher current densities for the MWNTs modified CP substrates upon closer observation, the inset of the first CV cycle in Figure 1a & 1c. This phenomenon might arise from two facts. On one hand, the monomer concentrations on the electrode/electrolyte interfacial could be enhanced greatly by the hydrogen bonding between the defects containing oxygen functional groups[41] or the -C-O-C, -COOH and -COOR groups on the MWNTs and the aniline monomers, which would give rise to higher oxidation current density. On the other hand, the oxidation of the functional groups[43] overlapped with the oxidation of the monomers, and therefore yielding more remarkable oxidation current densities in the initial stage of the electropolymerization process. Apart from the significantly different current density in the 1st CV cycle, difference in the potential of the cathodic peak in the negative scan is also observed. The reduction potential is found to be 0.403, 0.393, 0.383, and 0.389 V for the PANI-CP, PANI-AS, PANI-EC, and PANI-E, respectively. The functional groups which were oxidized in the positive scan might be responsible for the lowered potential required to reduce the electrode materials. The average surface coverage, Γ^*, of PANI polymers electrodeposited onto different substrates can be calculated according to Eq 1 and 2:[44]

$$\Gamma^* = Q/nFA \qquad [1]$$

$$Q = \frac{\int i\,dV}{2v} \qquad [2]$$

where Γ^* is the average surface coverage in mol/cm^2, Q is the total Faradic charges consumed during the electropolymerization calculated from the 15th CV cycle in C, n is the electron transfer number, 2.5,[45,46] F is Faraday constant (96485 C/mol), and A is the electrode area in cm^2, $\int i\,dV$ is the integrated area of the CV curve, and v is the scan rate in V/s. The Γ^* values of the PANI-CP, PANI-AS, PANI-EC, and PANI-E nanocomposite thin films are estimated to be 0.39, 0.44, 0.35, and 0.46 μmol/cm^2 using Eq 1 and 2. The lowest Γ^* found for the PANI-EC is due to the preferred nucleation growth resulted from the strong interactions between the hydrogen bonding via the -COOH groups in the MWNTs and the aniline monomers, which might induce some agglomerations during the film electropolymerization process.[47]

Structural and morphology characterization.— Figure 2 shows the morphology of the nanocomposite thin films. The nanocomposite thin films are observed to display different structure. For the PANI film grown onto carbon paper, the film shows an interesting flower-like growth pattern. As to the thin films grown onto MWNTs-coated carbon paper substrates, polymer nanoparticles can be observed besides the MWNTs embedded in the polymer matrix. PANI-EC thin film also exhibits some growth orientation, which further verifies the calculated lowest average surface coverage found in the film growth process.
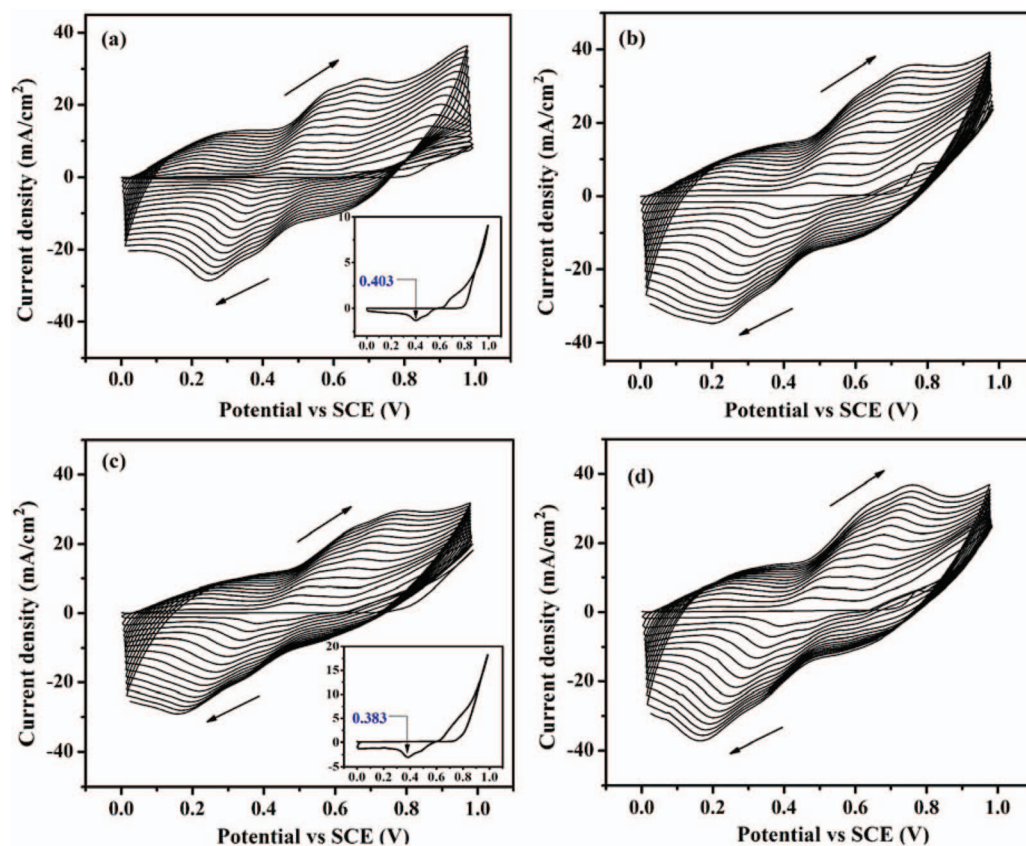
Figure 1. Electropolymerization synthesis of (a) PANI-CP, (b) PANI-AS, (c) PANI-EC, and (d) PANI-E at a scan rate of 50 mV/s in 1.0 M H$_2$SO$_4$ aqueous solution containing 0.1 M aniline monomers. The inset is the 1st CV cycle showing the irreversible oxidation of aniline.

Figure 3 depicts the FT-IR spectra of the nanocomposite thin films. In the pure PANI thin film grown onto carbon paper, the strong signals at 1549 and 1463 cm^{-1} correspond to the characteristic C $=$ C stretching mode of the quinoid and benzenoid rings, respectively,[48] suggesting an oxidation state of emeraldine salt state in the PANI polymer.[49] The peaks at 1100 and 857 cm^{-1} are assigned to the in-plane and out-of-plane bending of the C-H.[50,51] The peaks at 1291 and 1207 cm^{-1} are attributed to the C–N and C $=$ N stretching mode.[52,53]

All these peaks can also be found in the MWNTs/PANI nanocomposite thin films. It is worth noting that a remarkable blueshift of the peaks was observed for the PANI-EC film. A broad spectra around 3307 cm^{-1}, which originates from the stretching vibrations of the –OH group, verifies the –COOH functionalities in the PANI-EC film. The interactions between –COOH functional groups and the polymer matrix are believed to account for the spectrum changes, which is in good agreement with the results reported before.[36]
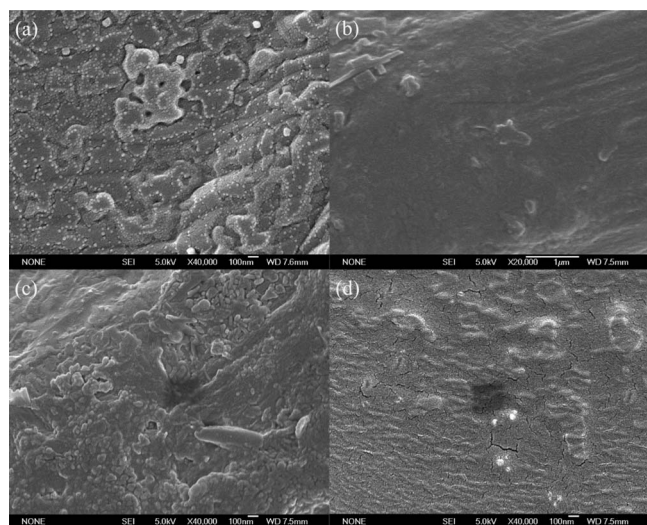
Figure 2. SEM images of nanocomposite thin films (a) PANI-CP, (b) PANI-AS, (c) PANI-EC, and (d) PANI-E, respectively.
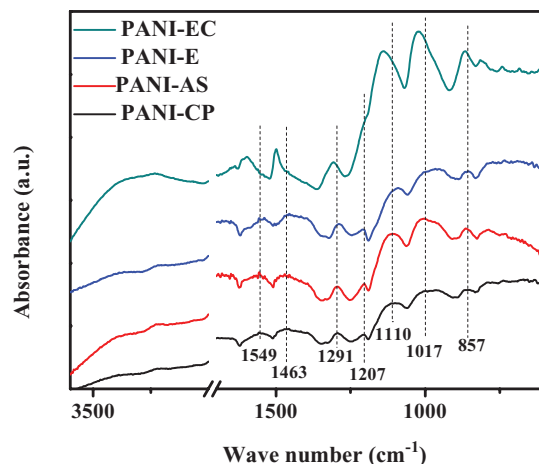
Figure 3. FT-IR spectra of PANI-CP, PANI-AS, PANI-EC, and PANI-E nanocomposite thin films.
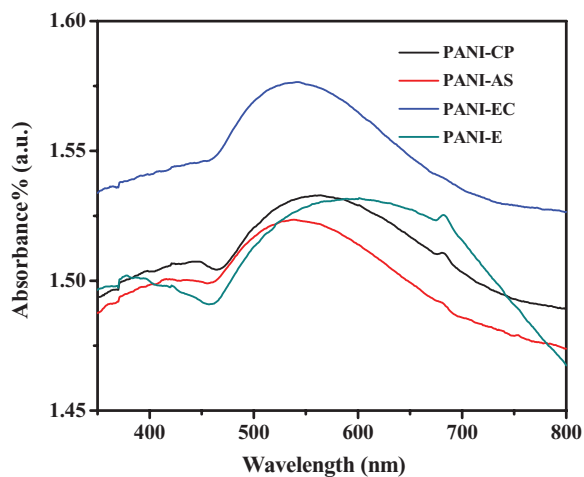
Figure 4. Diffuse reflectance absorption spectra of PANI-CP, PANI-AS, PANI-EC, and PANI-E nanocomposite thin films.

Optical properties and bandgap calculation.— Band gap (E_g), which governs the intrinsic electronic, optical and magnetic properties of materials, is of prime importance for semiconducting polymers.[54] The bandgap of the materials can be obtained by electrochemical methods, denoted as ($E_{g,EC}$), and photoelectron spectroscopy (PES), both of which also provide detailed information concerning the position of highest occupied molecular orbital (HOMO) and lowest unoccupied molecular orbital (LUMO) levels with respect to the vacuum level. Ultraviolet–visible spectroscopy is also commonly used to obtain the optical bandgap, denoted as E_g^{opt}, owing to its convenience, although it does not give exact HOMO or LUMO values of the material.[55] E_g^{opt} of the nanocomposite thin films was measured from the diffuse reflectance absorption spectra of the films using Eq 3:[56]

$$E_g^{opt} = \frac{1240}{\lambda_{edge}} \qquad [3]$$

where E_g^{opt} is the optical bandgap in eV and λ_{edge} is the absorption edge in nm. Figure 4 shows the diffuse reflectance absorption spectra of the thin films. The E_g^{opt} values of the PANI-CP, PANI-AS, PANI-EC, and PANI-E nanocomposite thin films are estimated to be 2.23, 2.31, 2.29, and 2.09 eV, respectively. The optical bandgap of PANI is usually dependent on its oxidation states, where the fully reduced and insulating form (leucoemeraldine base, LB) exhibits larger bandgap (higher than 3 eV) and the fully oxidized and semiconducting form (pernigraniline base, PNB) possess a lower bandgap (lower than 2 eV).[57] The band gaps of the nanocomposites are close to the reported value of 2.21 eV for the doped PANI in the emeraldine base (EB) form,[58] implying an oxidized state of the films. The difference in the bandgap of the nanocomposite thin films suggests a slight difference in the oxidation degree of the polymer matrix induced by the functional groups in the MWNTs.

Electrochemical characterization.— *Cyclic Voltammetry of the Nanocomposite Thin Films.*— Figure 5a–5e depicts the CV curves of the nanocomposite thin films at different scan rates. The redox peaks, indicating the typical pseudocapacitance characteristic of the PANI materials,[59,60] become more well-defined with decreasing the scan rate. At a larger scan rate of 100 mV/s, three pairs of redox peaks A/A', B/B' and D/D' can be observed while four redox peaks, A/A', B/B', C/C', and D/D' are evolved at smaller scan rate, i.e., 20 or 10 mV/s. A/A' and D/D' originate from the transition from leucoemeraldine salt (LS) to emeraldine salt (ES) and emeraldine salt (ES) to pernigraniline salt (PS), respectively.[61] The middle redox peaks, B/B' and C/C', are related to the existence of phenazine rings formed by a cross-linking reaction between polyamine chains or the insertion of nitreniumcations of aniline in the polymer matrix.[62]

Table I. Capacitances of the nanocomposite thin films at different scan rates.

Scan rate (mV/s)	Capacitance (mF/cm^2)			
	PANI-CP	PANI-AS	PANI/COOH	PANI/COOR
100	209.23	285.17	195.31	280.09
50	227.29	351.23	237.18	306.55
20	243.48	391.93	260.63	325.70
10	247.85	399.76	270.42	333.97

Interestingly, the first oxidation peaks of the nanocomposite thin films show a correlation with the bandgap, where the PANI-E and PANI-CP thin films with a lower E_g^{opt} exhibit a lower oxidation peak around 0.213 V and the PANI-EC and PANI-AS thin films exhibit a higher oxidation peak around 0.227 V in the positive sweeping. The thin films with a lower band gaps can be oxidized more easily requiring less energy when they are subjected to an external potential whereas it is more difficult for the films with high band gaps to be oxidized at higher voltage.

Table I lists the specific areal capacitance of nanocomposite films calculated from the corresponding CV curves at different scan rates from −0.2 to 0.8 V in 1.0 M H$_2$SO$_4$ aqueous solution using Eq 4:[63,64]

$$C_s = \left(\int i dV \right) / (2S \times \Delta V \times \nu) \qquad [4]$$

where C_s is the specific areal capacitance in F/cm^2, $\int i dV$ is the integrated area of the CV curve, S is the surface area of the active materials in the single electrode in cm^2, ΔV is the scanned potential window in V, and ν is the scan rate in V/s. The capacitances are four orders of magnitude higher than the areal capacitances of carbonaceous materials (10–40 μF/cm^2) and significantly superior to those most reported directly-grown pseudocapacitive nanostructural films (0.1–125 mF/cm^2).[27] Among these nanocomposite thin films, PANI-AS possesses the highest areal capacitances followed by PANI-E and PANI-EC, and PANI-CP exhibits the lowest capacitances. At a scan rate of 10 mV/s, the areal capacitance of PANI-AS, PANI-E, PANI-EC and PANI-CP is 399.76, 333.97, 270.42, and 247.85 mF/cm^2. The capacitance is increased by 61.3, 34.7, and 9.1% for PANI-AS, PANI-E, PANI-EC, respectively, when compared to that of PANI-CP. The synergistic effects between MWNTs and PANI are responsible for the enhancement of the capacitance.

The drop in the specific capacitance with increasing the scan rate is usually observed for the electrode materials owning to the slow ion diffusion and decreased utilization efficiency of the electrode materials with only relatively large pores penetrated into by ions at higher scan rates.[65–67] It is worth noting that the capacitance retention ratio[65] (the ratio of the capacitance obtained at 100 mV/s to the capacitance obtained at 5 mV/s) is 84.42, 71.34, 72.22 and 83.87% for the PANI-CP, PANI-AS, PANI-EC, and PANI-E nanocomposite films, respectively. This unusually high retention ratio is attributed to the large and accessible surface area of the nanocomposite thin films, whose exposed flat sheets facilitate the ion transport and enhance the transport rate in the material.[68] These values are much higher than those state-of-the-art carbonaceous materials and most pseudocapacitive nanostructure arrays.[27] Besides, the difference in the retention ratio among the nanocomposite films might lie in the morphology differences as confirmed by SEM images.[69] It's suggested the flower-like pattern in the PANI-CP film is more favorable for the ion transport than the nanoparticles in the PANI-AS film do.

Galvanostatic charge-discharge measurement.—The galvanostatic charge-discharge measurement is a reliable way to obtain the electrochemical capacitance of the materials under controlled current conditions. Galvanostatic charge-discharge measurements at different current densities by chronopotentiometry (CP) were carried out on the nanocomposite thin films in 1.0 M H$_2$SO$_4$ aqueous solution in a potential range from −0.2 to 0.8 V to evaluate the areal capacitances
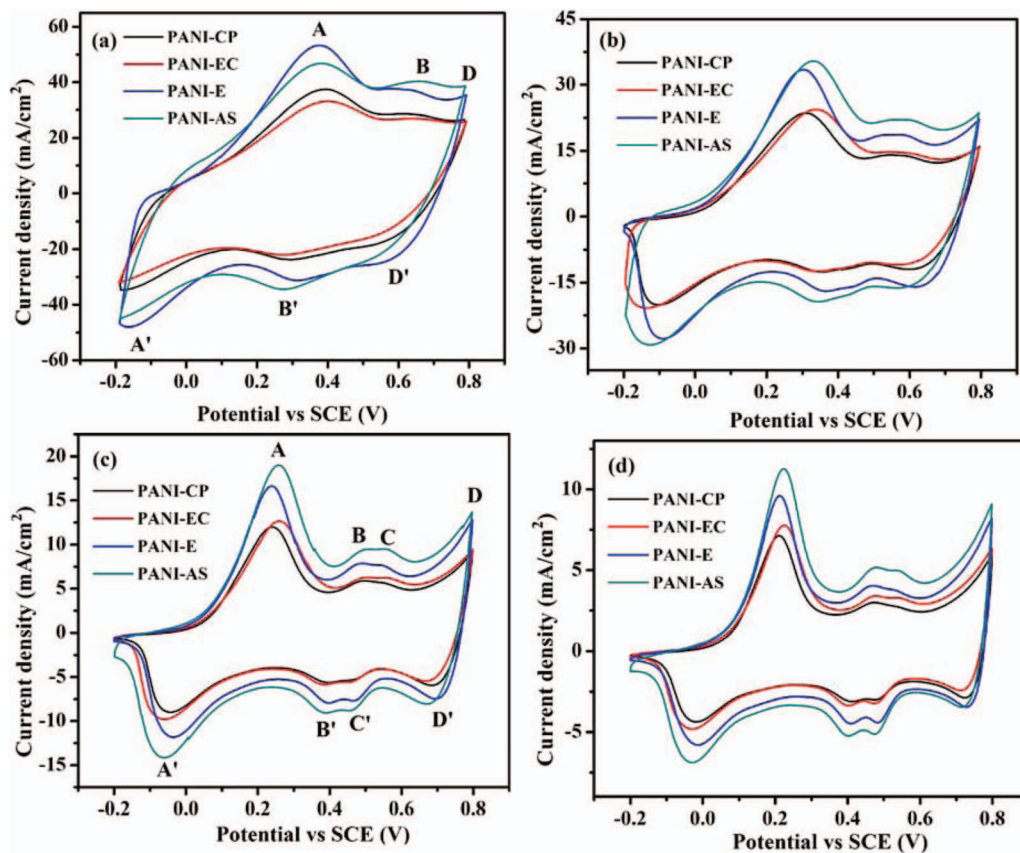
Figure 5. CV curves of the nanocomposite thin films at a scan rate of (a) 100, (b) 50, (c) 20, and (d) 10 mV/s, respectively, in in 1.0 M H$_2$SO$_4$ aqueous solution.

of the films using Eq 5:

$$C_s = (i \times t)/(S \times \Delta V) \qquad [5]$$

where C_s is the areal capacitance in F/cm^2, i is the discharge current in A, t is the discharge time in s, S is the surface area of the active materials in the single electrode in cm^2, and ΔV is the scanned potential window (excluding IR drop in the beginning of the discharge process) in V. Figure 6 shows the potential responses of the nanocomposite thin films at a current density of 15 mA/cm^2.
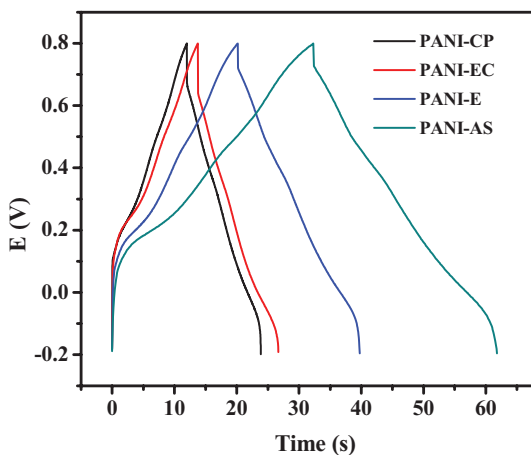
Figure 6. Charge-discharge curves at a current density of 15 mA/cm^2 of PANI-CP, PANI-AS, PANI-EC, and PANI-E nanocomposite thin films under a potential range from −0.2 to 0.8 V in 1.0 M H$_2$SO$_4$ aqueous solution.

The energy density, E, and the power density, P, were calculated from Eq 6 and 7:[27,36]

$$E = \frac{\frac{1}{2}C_s \Delta V^2}{3600} \qquad [6]$$

$$P = \frac{3600E}{t} \qquad [7]$$

where E is the areal energy density in Wh/cm^2, P is the areal power density in W/cm^2. C_s is the areal capacitance in F/cm^2, ΔV is the scanned potential window (excluding IR drop in the beginning of the discharge) in V, t is the discharge time in s. The coulombic efficiency, η, can be calculated according to Eq 8:[70]

$$\eta = \left(\frac{t_D}{t_C}\right) \times 100 \qquad [8]$$

where t_D and t_C are discharging and charging time, respectively.

The capacitances, energy densities, power densities, and coulombic efficiencies at a current density of 20, 15 and 10 mA/cm^2 are presented in Table II. Consistent with the CV results, PANI-AS is found to have the highest areal capacitances and energy densities followed by PANI-E, PANI-EC, and PANI-CP. The capacitance values obtained are very close to those obtained from CV results. Even at a high current density of 20 mA/cm^2, the energy density can reach as high as more than 30 μWh/cm^2 at a power density of around 8 mW/cm^2, compared to ~2.52 μWh/cm^2 at a power density of 0.01 mW/cm^2 for the graphite oxide/PANI nanocomposite thin films in the previous study.[36] The coulombic efficiencies of the nanocompoiste thin films are also very high, reaching 99.0% at a current density of 20 mA/cm^2, indicating the nanocomposite thin films suitable for supercapacitors applications.

Table II. Energy densities, power densities, capacitances, and coulombic efficiencies of the nanocomposite thin film at different current densities of 20, 15, and 10 mA/cm^2.

Current density (A/g)		PANI-CP	PANI-EC	PANI-E	PANI-AS
	E (mWh/cm^2)	20.18	20.29	32.62	34.2
20	P (W/cm^2)	8.37	7.87	8.65	8.66
	Cs (mF/ cm^2)	207.41	235.83	279.44	328.01
	η	99.0%	95.1%	97.0%	96.2%
	E (mWh/cm^2)	21.74	22.35	32.39	35.36
15	P (W/cm^2)	6.59	6.24	6.76	6.61
	Cs (mF/ cm^2)	202.56	232.72	274.29	327.46
	η	99.0%	93.8%	97.4%	94.3%
	E (mWh/cm^2)	23.24	24.59	24.59	37.70
10	P (W/cm^2)	4.58	4.39	4.78	4.62
	Cs (mF/ cm^2)	193.63	229.31	265.05	318.46
	η	98.0%	91.9%	95.3%	91.0%
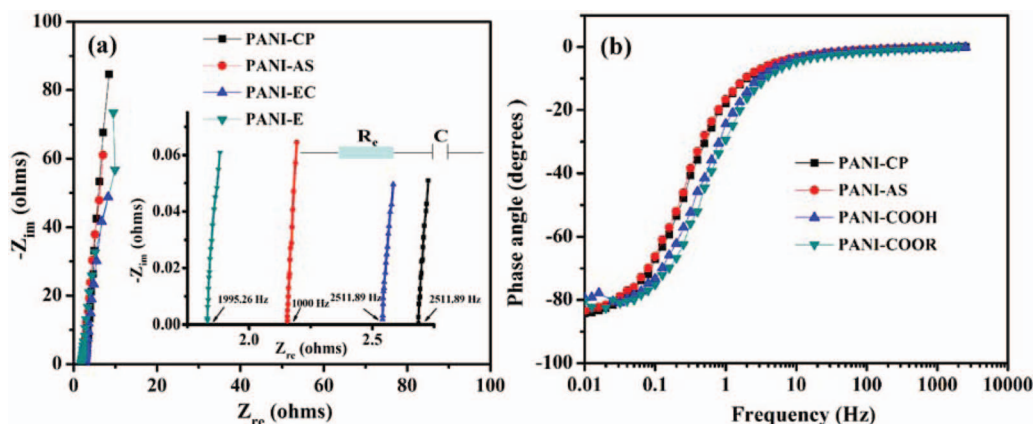
Figure 7. Complex plane plots of PANI-CP, PANI-AS, PANI-EC, and PANI-E nanocomposite thin films. The inset is an expand view of the Nyquist plot at the high frequency region and the equivalent circuit of the anncomposite films.

Electrochemical impedance spectroscopy (EIS).—To obtain a further fundamental understanding of the properties of the electrode materials, EIS was employed and the corresponding complex plane plots are shown in Figure 7. The excellent capacitance performance can be clearly observed with the nanocomposite thin films approaching an almost vertical line. No resistor-capacitor (RC) loops or semicircles appear in the high frequency region, indicating a negligible charge resistance.[71] The Warburg resistance (diffusion impedance), that is, the 45° portion of the Nyquist plots (left part of Figure 7) in the middle frequency region, is negligible for the thin films, suggesting a short ion diffusion path and low ion diffusion resistance, thus a better charge propagation and ion response time.[72] The phase angle of the thin films is close to −90° in the low frequency region, implying an ideal capacitor functionality.[63] The characteristic frequency f_o for a phase angle of −45° marks the point, at which the resistive and capacitive impedances are equal.[73] Table III lists f_o and the corresponding time constant τ_o ($= 1/f_o$) of the thin films. As seen from the Table, the τ_o of PANI-CP and PANI-AS is about the same, 4.0 s, while shorter τ_o is found to be 2.5 and 2.0 s for PANI-EC, and PANI-E. The rapid frequency response can be accounted for the large and accessible surface area, whose exposed flat sheets enhance the ion transport rate in the material.[68]

The equivalent series resistance (ESR, R_e), which mainly arises from the electrolyte, intrinsic resistance of the active material and contact resistance at the active material/current collector interface, is 2.833, 2.655, 2.542, and 1.832 Ω for the PANI-CP, PANI-AS, PANI-EC, and PANI-E thin film, respectively. Heteroatoms and functional groups are reported to be capable of improving the electrochemical performances by increasing the wettability or decreasing the resistivity of the electrodes.[74,75] Therefore, The reduced ESR is inferred to be brought by the defects in the as-received MWNTs or the -C-O-C, -COOH, and -COOR functional groups in the modified MWNTs, which are expected to decrease the surface resistivity of the electrode.[76] Equivalent circuit consisting of a combined resistance R_e and a capacitance C from the PANI film is proposed and the fitting paprameters are listed in Table IV.

Stability of the nanocomposite thin films.— The instability of the capacitors based on conductive polymer films (especially for PANI) during long term charge/discharge cycling is one of the biggest concerns. Therefore, the stability of the nanocomposite thin films is investigated. Figure 8 depicts the capacitance retention of the nanocomposite thin films at a current density of 50 mA/cm^2 during 1000 cycles. It can be observed that the PANI-CP retains 85% of capacitance after 1000 cycles while the values for the nanocomposite thin films grown onto as-received or modified MWNTs are slightly lower than 80%. It's inferred that more complete redox reactions in the MWNTs/PANI nanocomposite thin films may result in a more severe expanding and shrinking of the PANI matrix, thus giving rise to more obvious degradation of the electrode material.

Table III. f_o and τ_o of the nanocomposite thin films obtained from EIS data.

	PANI-CP	PANI-AS	PANI-EC	PANI-E
f_o(Hz)	0.25	0.25	0.40	0.50
τ_o(s)	4.00	4.00	2.50	2.00

Table IV. Fitting parameters of the nanocomposite thin films from the fitting.

	PANI-CP	PANI-AS	PANI-EC	PANI-E
R_e (Ω)	2.833 ± 0.025	1. 2.265 ± 0.022	2.656 ± 0.025	1.942 ± 0.065
C (F)	0.1852 ± 0.0026	0.2546 ± 0.0038	0.1293 ± 0.0020	0.1132 ± 0.0051
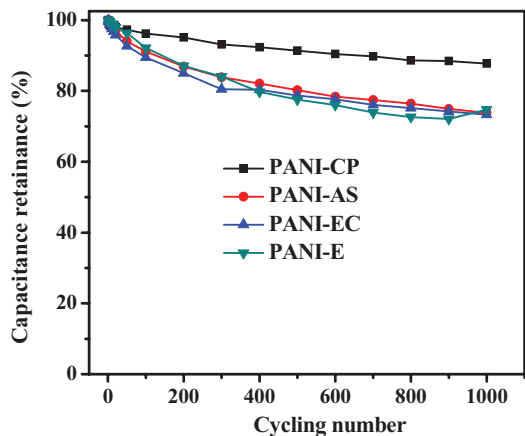
Figure 8. Capacitance retention of the nanocomposite thin films as a function of cycling number.

Conclusions

Free-standing polyaniline (PANI) nanocomposite thin films from as-received MWNTs or modified MWNTs with C-O-C- and –COOH or –COOR functionalities have been prepared via electropolymerization approach. The free-standing nanocomposite thin films were used as supercapacitor electrodes and the electrochemical performances were evaluated. The nanocomposite thin films from the MWNTs exhibit enhanced capacitances and energy densities due to the interactions between the defects or –COOH and C-O-C- or –COOR functionalities in the MWNTs and PANI matrix. Equivalent circuit consisting of a combined resistance and a capacitor is successfully fitted with the EIS data. High capacitance retention (around 80%) after 1000 charge/discharge recycles is also obtained for the films. The facile preparation and excellent capacitive properties making these nanocomposite thin films from MWNTs and PANI highly promising as supercapacitors materials in the future.

Acknowledgments

References

1. P. Simon and Y. Gogotsi, *Nat. Mater.*, **7**, 845 (2008).
2. M. Jayalakshmi and K. Balasubramanian, *Int. J. Electrochem. Sci.*, **3**, 119 (2008).
3. C. Yuan, B. Gao, L. Shen, S. Yang, L. Hao, X. Lu, F. Zhang, L. Zhang, and X. Zhang, *Nanoscale*, **3**, 529 (2011).
4. Y. Zhang, H. Feng, X. Wu, L. Wang, A. Zhang, T. Xia, H. Dong, X. Li, and L. Zhang, *Int. J. Hydrogen Energy*, **34**, 4889 (2009).
5. D. Cericola and R. Kötz, *Electrochim. Acta*, **72**, 1 (2012).
6. S. W. Lee, B. M. Gallant, H. R. Byon, P. T. Hammond, and Y. Shao-Horn, *Energy Environ. Sci.*, **4**, 1972 (2011).
7. R. Kötz and M. Carlen, *Electrochim. Acta*, **45**, 2483 (2000).
8. O. Barbieri, M. Hahn, A. Herzog, and R. Kötz, *Carbon*, **43**, 1303 (2005).
9. Z. Tai, X. Yan, J. Lang, and Q. Xue, *J. Power Sources*, **199**, 373 (2011).
10. D. A. C. Brownson, D. K. Kampouris, and C. E. Banks, *J. Power Sources*, **196**, 4873 (2011).
11. Y. Zhu, S. Murali, M. D. Stoller, K. Ganesh, W. Cai, P. J. Ferreira, A. Pirkle, R. M. Wallace, K. A. Cychosz, and M. Thommes, *Science*, **332**, 1537 (2011).
12. J. R. Miller and P. Simon, *Science*, **321**, 651 (2008).
13. J. Li, X. Cheng, A. Shashurin, and M. Keidar, *Graphene*, **1**, 1 (2012).
14. A. Shukla, S. Sampath, and K. Vijayamohanan, *Curr. Sci.*, **79**, 1656 (2000).
15. G. Yu, L. Hu, M. Vosgueritchian, H. Wang, X. Xie, J. R. McDonough, X. Cui, Y. Cui, and Z. Bao, *Nano Lett.*, **11**, 2905 (2011).
16. Z. S. Wu, D. W. Wang, W. Ren, J. Zhao, G. Zhou, F. Li, and H. M. Cheng, *Adv. Funct. Mater.*, **20**, 3595 (2010).
17. T. Brezesinski, J. Wang, S. H. Tolbert, and B. Dunn, *Nat. Mater.*, **9**, 146 (2010).
18. X. Xia, J. Tu, Y. Zhang, X. Wang, C. Gu, X. Zhao, and H. J. Fan, *ACS nano*, **6**, 5531 (2012).
19. Y. Yang, D. Kim, M. Yang, and P. Schmuki, *Chem. Commun.*, **47**, 7746 (2011).
20. J. De Girolamo, P. Reiss, M. Zagorska, R. De Bettignies, S. Bailly, J. Y. Mevellec, S. Lefrant, J. P. Travers, and A. Pron, *Phys. Chem. Chem. Phys.*, **10**, 4027 (2008).
21. D. Aldakov, T. Jiu, M. Zagorska, R. de Bettignies, P. H. Jouneau, A. Pron, and F. Chandezon, *Phys. Chem. Chem. Phys.*, **12**, 7497 (2010).
22. J. Zhu, S. Wei, L. Zhang, Y. Mao, J. Ryu, P. Mavinakuli, A. B. Karki, D. P. Young, and Z. Guo, *J. Phys. Chem. C*, **114**, 16335 (2010).
23. K. Ding, H. Jia, S. Wei, and Z. Guo, *Ind. Eng. Chem. Res.*, **50**, 7077 (2011).
24. H. Wei, X. Yan, Y. Li, S. Wu, A. Wang, S. Wei, and Z. Guo, *J. Phys. Chem. C*, **116**, 4500 (2012).
25. H. Wei, X. Yan, Y. Li, H. Gu, S. Wu, K. Ding, S. Wei, and Z. Guo, *J. Phys. Chem. C*, **116**, 16286 (2012).
26. G. Wang, L. Zhang, and J. Zhang, *Chem. Soc. Rev.*, **41**, 797 (2012).
27. J. Liu, J. Jiang, M. Bosman, and H. J. Fan, *J. Mater. Chem.*, **22**, 2419 (2012).
28. Y. Y. Horng, Y. C. Lu, Y. K. Hsu, C. C. Chen, L. C. Chen, and K. H. Chen, *J. Power Sources*, **195**, 4418 (2010).
29. R. Ramya, R. Sivasubramanian, and M. Sangaranarayanan, *Electrochim. Acta*, in press (2012).
30. G. Zotti, S. Cattarin, and N. Comisso, *J. Electroanal. Chem. Interfacial Electrochem.*, **239**, 387 (1988).
31. X. X. Liu, L. Zhang, Y. B. Li, L. J. Bian, Z. Su, and L. J. Zhang, *J. Mater. Sci.*, **40**, 4511 (2005).
32. J. Zhu, H. Gu, Z. Luo, N. Haldolaarachige, D. P. Young, S. Wei, and Z. Guo, *Langmuir*, **28**, 10246 (2012).
33. H. Gu, S. Tadakamalla, Y. Huang, H. A. Colorado, Z. Luo, N. Haldolaarachchige, D. P. Young, S. Wei, and Z. Guo, *ACS Appl. Mater. Interfaces*, **4**, 5613 (2012).
34. T. Osaka, T. Nakajima, K. Naoi, and B. B. Owens, *J. Electrochem. Soc.*, **137**, 2139 (1990).
35. H. Wei, X. Yan, S. Wu, Z. Luo, S. Wei, and Z. Guo, *J. Phys. Chem. C*, **116**(47), 25052 (2012).
36. H. Wei, J. Zhu, S. Wu, S. Wei, and Z. Guo, *Polymer*, **54**(7), 1820 (2013).
37. J. Li, X. Cheng, A. Shashurin, and M. Keidar, *Graphene*, **1**, 1 (2012).
38. B. Dong, B.-L. He, C.-L. Xu, and H.-L. Li, *Mater. Sci. Eng., B*, **143**, 7 (2007).
39. Z. Niu, P. Luan, Q. Shao, H. Dong, J. Li, J. Chen, D. Zhao, L. Cai, W. Zhou, and X. Chen, *Energy Environ. Sci.*, **5**, 8726 (2012).
40. V. Khomenko, E. Frackowiak, and F. Beguin, *Electrochim. Acta*, **50**, 2499 (2005).
41. H. Gu, S. B. Rapole, Y. Huang, D. Cao, Z. Luo, S. Wei, and Z. Guo, *J. Mater. Chem. A*, **1**, 2011 (2013).
42. C. Buron, B. Lakard, A. Monnin, V. Moutarlier, and S. Lakard, *Synth. Met.*, **161**, 2162 (2011).
43. H. Luo, Z. Shi, N. Li, Z. Gu, and Q. Zhuang, *Anal. Chem.*, **73**, 915 (2001).
44. X. M. Feng, R. M. Li, Y. W. Ma, R. F. Chen, N. E. Shi, Q. L. Fan, and W. Huang, *Adv. Funct. Mater.*, **21**, 2989 (2011).
45. C. Peng, D. Hu, and G. Z. Chen, *Chem. Commun.*, **47**, 4105 (2011).
46. A. R. Elkais, M. M. Gvozdenović, B. Z. Jugović, J. S. Stevanović, N. D. Nikolić, and B. N. Grgur, *Prog. Org. Coat.*, **71**, 32 (2011).
47. M. N. Hyder, S. W. Lee, F. C. Cebeci, D. J. Schmidt, Y. Shao-Horn, and P. T. Hammond, *ACS nano*, **5**, 8552 (2011).
48. A. Kellenberger, E. Dmitrieva, and L. Dunsch, *J. Phys. Chem. B*, **116**, 4377 (2012).
49. S. Quillard, G. Louarn, S. Lefrant, and A. MacDiarmid, *Phys. Rev. B*, **50**, 12496 (1994).
50. W. A. El-Said, C. H. Yea, J. W. Choi, and I. K. Kwon, *Thin Solid Films*, **518**, 661 (2009).
51. J. Zhu, S. Wei, L. Zhang, Y. Mao, J. Ryu, N. Haldolaarachchige, D. P. Young, and Z. Guo, *J. Mater. Chem.*, **21**, 3952 (2011).
52. Y. Li, X. Zhao, Q. Xu, Q. Zhang, and D. Chen, *Langmuir*, **27**, 6458 (2011).
53. H. Gu, Y. Huang, X. Zhang, Q. Wang, J. Zhu, L. Shao, N. Haldolaarachchige, D. P. Young, S. Wei, and Z. Guo, *Polymer*, **53**, 801 (2011).
54. S. A. Jenekhe, *Nature*, **322**, 345 (1986).
55. P. Reiss, E. Couderc, J. De Girolamo, and A. Pron, *Nanoscale*, **3**, 446 (2011).
56. C. Bora and S. Dolui, *Polymer*, **53**, 923 (2012).
57. O. Kwon and M. L. McKee, *J. Phys. Chem. B*, **104**, (2000).
58. H. S. Abdulla and A. I. Abbo, *Int. J. Electrochem. Sci.*, **7**, 10666 (2012).
59. A. Rudge, J. Davey, I. Raistrick, S. Gottesfeld, and J. P. Ferraris, *J. Power Sources*, **47**, 89 (1994).
60. F. Fusalba, P. Gouérec, D. Villers, and D. Bélanger, *J. Electrochem. Soc.*, **148**, A1 (2001).

61. Y. G. Wang, H. Q. Li, and Y. Y. Xia, *Advanced Materials*, **18**, 2619 (2006).
62. E. Genies, M. Lapkowski, and J. Penneau, *J. Electroanal. Chem. Interfacial Electrochem.*, **249**, 97 (1988).
63. J. Zhu, M. Chen, H. Qu, Z. Luo, S. Wu, H. A. Colorado, S. Wei, and Z. Guo, *Energy Environ. Sci.*, **50**, 3210 (2013).
64. J. Zhu, M. Chen, H. Qu, X. Zhang, H. Wei, Z. Luo, H. A. Colorado, S. Wei, and Z. Guo, *Polymer*, **53**, 5953 (2012).
65. Z. L. Wang, R. Guo, G. R. Li, H. L. Lu, Z. Q. Liu, F. M. Xiao, M. Zhang, and Y. X. Tong, *J. Mater. Chem.*, **22**, 2401 (2012).
66. J. Yan, E. Khoo, A. Sumboja, and P. S. Lee, *ACS Nano*, **4**, 4247 (2010).
67. W. Xing, S. Qiao, R. Ding, F. Li, G. Lu, Z. Yan, and H. Cheng, *Carbon*, **44**, 216 (2006).
68. M. F. El-Kady, V. Strong, S. Dubin, and R. B. Kaner, *Science*, **335**, 1326 (2012).
69. L. L. Zhang, S. Zhao, X. N. Tian, and X. Zhao, *Langmuir*, **26**, 17624 (2010).
70. L. J. Sun, X. X. Liu, K. K. T. Lau, L. Chen, and W. M. Gu, *Electrochim. Acta*, **53**, 3036 (2008).
71. C. Xiang, M. Li, M. Zhi, A. Manivannan, and N. Wu, *J. Mater. Chem.*, **22**, 19161 (2012).
72. R. I. Jafri, A. K. Mishra, and S. Ramaprabhu, *J. Mater. Chem.*, **21**, 17601 (2011).
73. P. Taberna, P. Simon, and J.-F. Fauvarque, *J. Electrochem. Soc.*, **150**, A292 (2003).
74. D. Hulicova, M. Kodama, and H. Hatori, *Chem. Mater.*, **18**, 2318 (2006).
75. G. Lota, K. Lota, and E. Frackowiak, *Electrochem. Commun.*, **9**, 1828 (2007).
76. J. Shen, A. Liu, Y. Tu, G. Foo, C. Yeo, M. B. Chan-Park, R. Jiang, and Y. Chen, *Energy Environ. Sci.*, **4**, 4220 (2011).